Available online at www.sciencedirect.com
ScienceDirect
Journal of Power Sources 165 (2007) 874–879
JOURNAL OF POWER SOURCES
www.elsevier.com/locate/jpowsour

Short communication

Design criteria for nanostructured Li-ion batteries

K.E. Aifantis [a,*], S.A. Hackney [b], J.P. Dempsey [c]

[a] *Materials Science Center, Ecole des Mines, France*
[b] *Department of Materials Science and Engineering, Michigan Technological University, USA*
[c] *Department of Civil & Environmental Engineering, Clarkson University, USA*

Received 25 July 2006; received in revised form 17 October 2006; accepted 24 October 2006
Available online 6 February 2007

Abstract

Extensive experimental research has indicated that active/inactive nanocomposites are promising electrode materials for rechargeable Li-ion batteries. Nanocomposite anode materials allow for capacities between 900 and 4000 mAh g^{-1} whereas graphitic anodes, which are currently being used by industry, allow for a much lower capacity of 372 mAh g^{-1}. By treating the active sites (which may be comprised of Si, Sn, Al, or Bi) as nanospheres embedded in an inert matrix, linear elastic fracture mechanics are employed in order to develop design criteria for these alternative battery systems, with respect to fracture that results from the large volume expansions that the active sites undergo upon Li-insertion. In particular, the present study: (i) predicts that smaller active site volume fractions are more stable; (ii) Griffith's criterion is used to estimate the crack radius at which cracking will stop; (iii) based on the ultimate tensile strength of the inactive matrix the critical crack length at which the electrode will fracture is calculated; (iv) a theoretical estimation is made for the size of the active sites that will not allow cracks to develop and hence fracture of the electrode will be prevented. Based on the above analysis, Si active sites allow for a greater anode lifetime and therefore are preferred over Sn, furthermore the formulation can be applied to determine the most appropriate matrix materials.

Keywords: Active/inactive nanocomposites; Linear elasticity; Critical energy release rate

1. Introduction

Lithium ion batteries are the main energy sources used in electronic devices such as cell phones and lap top computers, as well as in biomedical implantable devices. They are preferred over other battery chemistries, such as nickel–cadmium and nickel-metal-hydride, not only because they are non-toxic, but also because their high energy density reduces their weight by half and their volume by 20–50%. Initially, both the cathode and anode were comprised of lithium metal but this resulted in safety issues, and therefore since the 1990s graphite is being solely used as the anode. Graphite, though, has a very low Li atomic density at full Li capacity in the carbon intercalation compound (LiC_6), hence the volumetric Li capacity is rather low. This is an important aspect in choosing the electrode materials because the total amount of Li-ions that can be taken up by the electrode material corresponds to the total time integration of the battery current. Therefore extensive research is being performed for the development of alternative anode materials that would give a higher energy density for the Li-ion battery systems. Some experimental research indicates that promising candidates for next generation Li-ion negative electrodes are engineered materials exhibiting a micro- or nano-scale composite structure. This concept was originally suggested by Wang et al. [1] and later experimentally confirmed by Courtney and Dahn [2] and Thackeray et al. [3]. These nanocomposites are composed of materials capable of forming Li rich compounds (active materials) surrounded by a matrix material that is inert with respect to Li (inactive material). The matrix acts as a Li ion conductor while protecting the active sites from detrimental chemical reactions with the electrolyte. Both Si and Sn are good candidates for the active material in the composite structures as they have a very high Li intercalation density per host atom, forming the compounds $Li_{4.4}Si$ and $Li_{4.4}Sn$. In terms of the total time integrated battery current per mass, these compounds have capacities of 900 and 4000 mAh g^{-1}, respectively [4], whereas graphitic carbon gives a much lower Li capacity of 372 mAh g^{-1} [5] (it should be mentioned here that Si and Sn react with Li in a

* Corresponding author. Tel.: +30 6936 208504; fax: +30 2310 995921.
E-mail address: k.aifantis@mom.gen.auth.gr (K.E. Aifantis).

0378-7753/$ – see front matter © 2007 Published by Elsevier B.V.
doi:10.1016/j.jpowsour.2006.10.070

similar way that C does). The drawback, however, is that during maximum Li insertion Si suffers a 310% volume increase [4]; in fact all metals that can act as active sites such as Sn, Bi, Al exhibit over a 100% volume increase after Li alloy formation. As a result significant internal stresses are produced and during the initial electrochemical cycles loss of mechanical integrity takes place at the active site/matrix interface; this leads to fracture of the electrode and a loss of electrical integrity [4].

From the aforementioned it can be seen that it is essential to model these alternative anode configurations from a mechanics point of view, before they can be used commercially. First steps towards this direction have been taken (i) by Aifantis and Hackney [6] who examined the elastic internal stresses the nanocomposite electrode materials undergo upon charging and discharging, and (ii) by Aifantis and Dempsey [7] who predicted the stability of the anodes upon maximum Li insertion. In particular, in Ref. [7] various electrode configurations (disk-like active sites, fiber-like active sites, and spherical active sites) that are in the experimental stage were examined by employing linear elastic fracture mechanics. It was shown that spherical active sites allowed for the most stable behavior, and therefore only this configuration will be examined in the present work. Specifically, after determining the energy released during cracking as a function of the crack propagation distance, an expression is obtained for the stability index which allows the determination of the most stable active site volume fractions. Furthermore, Griffith's criterion is used to estimate the crack radius at which crack growth will stop, while the critical crack length at which fracture of the electrode takes place will also be determined. Finally, by considering some additional physics, the size of the active sites that will result in no cracking will be predicted.

2. Electrode configuration

The configuration of the problem at hand is shown in Fig. 1. It should be noted here that the crumbling effect at the active site/matrix interface is significantly reduced for active sites that have nanometre dimensions, such as spherical nanocrystalline Si particles with a 10 nm radius [5]. Additionally, this miniaturization is very effective from an electrochemical point of view since bulk Si reacts with Li at very large temperatures (400 K), whereas nanocrystalline Si can form Li alloys at room temperature [8].

It should also be noted that the capacity of bulk Si is significantly reduced after a few cycles [9], whereas at the nanorange it is closer to its theoretical value; i.e. 3000 mAh g^{-1} have been achieved for 40 nm thin films, after 25 cycles [10]. Based on this experimental background the anode is taken to be comprised of Si nanospheres embedded in an inert, with respect to Li, matrix. The resulting analysis will provide criteria towards the selection of the most appropriate matrix material.

As was mentioned in the introduction after the first few electrochemical cycles crumbling occurs at the Si/matrix interface. Since the matrix is more brittle from the Si it is assumed that it crumbles and forms a damage zone, as shown in Fig. 2. Since this region is severely damaged it is assumed to support only radial stresses (all other stress components vanish in that region), and

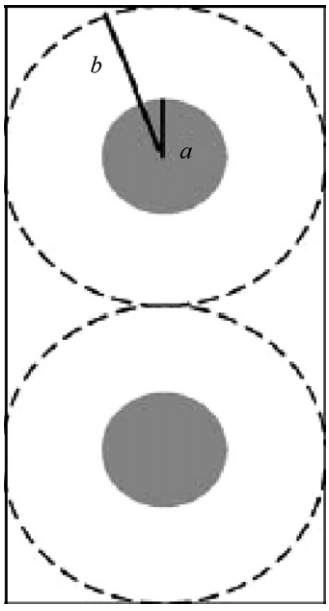

Fig. 1. Electrode configuration: spherical active sites (shaded) of radius a are embedded in an inert matrix (blank) of radius b. This figure depicts two unit cells.

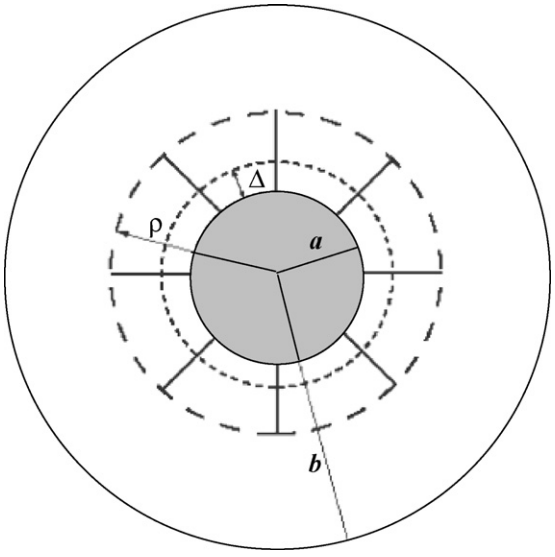

Fig. 2. Configuration of unit cell used in analysis; a and b are the radii of the active site and matrix, Δ is the free expansion of the active site if it were not constrained by the matrix, ρ is the crack radius.

can therefore be approximated by a number of radial cracks with length ρ–a. Furthermore, it should be noted that in Fig. 2, a and b are the radii of the Si and matrix, while Δ is the radial displacement to which the Si would expand to if it were not surrounded by the matrix.

3. Energy released during crack growth

The following formulation is a summary of the work in Ref. [7]. Upon electrochemical cycling an exchange of Li-ions takes place between the two electrodes. Upon charging of the battery Li-ions from the cathode are attracted to the negative electrode

and diffuse into the active sites, which as a result experience a 300% expansion, while upon discharging Li-ions return to the positive electrode. Since this study is concerned with fracture of the anode the following analysis is valid once maximum charging has been achieved. Upon maximum Li-insertion the stress that the Li-ions exert inside the active site is constant and therefore the pressure that the active site exerts onto the matrix is also constant and is set equal to p. Similarly the pressure that is exerted onto the unit cell under examination by a neighbouring cell is constant and set equal to q. This implies the conditions:

$$\sigma_{rr}(a) = -p, \qquad \sigma_{rr}(b) = -q \tag{1}$$

where σ_{rr} is the radial stress.

Since conditions of spherical symmetry are present the stress and displacement expressions in the active site can be written as

$$\sigma_{rr} = \sigma_{\theta\theta} = \sigma_{\phi\phi} = 2\frac{1+v_s}{1-2v_s}D_s; \qquad u_r = \frac{2(1+v_s)r}{E_s}D_s \tag{2}$$

where σ_{rr}, $\sigma_{\theta\theta}$, $\sigma_{\phi\phi}$ are the stresses in the r-, θ- and ϕ-directions respectively, furthermore in Eq. (2) r is the radial distance from the center of the active site, u_r is the displacement in the radial direction, v_s denotes the active site Poisson ratio, E_s the elastic modulus of the active site, and D_s is an integration constant to be determined from the boundary conditions. It can be seen that there is no stress variation in the r-direction since the stress in the active sites is uniform.

Considering Eqs. (1) with (2) allows the displacement inside the active site to be expressed as

$$u_r = -\frac{(1-2v_s)rp}{E_s}. \tag{3}$$

Now we can proceed to develop a displacement condition at the active site/matrix interface. If the active site was not surrounded by the matrix it would attain a radius of $r = a + \Delta$, upon maximum Li-insertion. For the present confined configuration, however, the surrounding matrix opposes this free expansion by pushing back the active site by a distance $-\delta$. It can therefore be said that the initial radius of the active site is $r_i = a + \Delta$, while the final radius of the active site, due to the presence of the matrix, is $r_f = a + \Delta - \delta$. Thus, the total displacement of the active particle surface, upon maximum Li-insertion, is $u_r = r_f - r_i = -\delta$:

$$u_r(a+\Delta) = -\delta = -\frac{(1-2v_s)(r+a)p}{E_s}. \tag{4}$$

Similarly the displacement at the active site/matrix interface can be formulated by considering the initial inner radius of the matrix annulus, wich is $r = a$ and that which it attains after maximum Li-insertion which is $r = a + \Delta - \delta$, according to the previous reasoning. Therefore at the active site/matrix interface $(r = a) u_r = \Delta - \delta$. Combining this boundary condition with Eq. (4) gives

$$u_r(a) = \Delta - \delta = \Delta - \frac{(1-2v_s)(\Delta + a)p}{E_s}. \tag{5}$$

In the sequel the stress and displacement expressions inside the next region of Fig. 2, which is the damage zone will be developed. Since this region is severely damaged such that it can support only radial stresses, the stress equibrium relation gives

$$\frac{d\sigma_{rr}}{dr} + \frac{2\sigma_{rr}}{r} = 0 \Rightarrow \sigma_{rr}(r) = \frac{k}{r^2}, \quad \text{for } a \le r \le \rho. \tag{6}$$

The integration constant, k, can be found by combining Eqs. (6) with (1), hence $k = -pa^2$. Furthermore, from Eq. (6) the displacement expression is found as

$$\sigma_{rr}(r) = E_g\frac{du_r}{dr} \Rightarrow \frac{du_r}{dr} = -\frac{pa^2}{E_g r^2} \Rightarrow u_r(r) = \frac{pa^2}{E_g r} + u^* \tag{7}$$

where E_g is the elastic modulus of the matrix.

The constant of integration u^* is found by setting the displacement right in front of the crack tip $u_+(\rho)$ equal to $u_r(\rho)$, hence

$$u_+(\rho) = u_r(\rho) = \frac{pa^2}{E_g\rho} + u^* \Rightarrow u^* = u_+(\rho) - \frac{pa^2}{E_g\rho} \tag{8}$$

where ρ is the distance from the centre of the active site to the crack tip, i.e. it is the crack radius.

Insertion now of Eq. (8) into Eq. (7) gives the displacement expression inside the damage zone as

$$u_r(r) = \frac{pa^2}{E_g}\left(\frac{1}{r} - \frac{1}{\rho}\right) + u_+(\rho), \quad \text{for } a \le r \le \rho. \tag{9}$$

Finally, the displacement expression in the third region of Fig. 2, i.e. inside the uncracked matrix, can be found by treating the matrix as a hollow sphere which experiences an internal pressure (by the active site) and an external pressure (by the neighboring unit cell). In fact, the solution for such a configuration has been solved by Westergard [11], and it reads

$$u_+(r) = \frac{r(1+v_g)}{E_g}\left\{p_*\frac{b^3/(2r^3) + (1-2v_g)(1+v_g)}{b^3/\rho^3 - 1} - q\frac{\rho^3/(2r^3) + (1-2v_g)(1+v_g)}{1-\rho^3/b^3}\right\}, \quad \text{for } \rho \le r \le b. \tag{10}$$

The internal pressure p_* is the pressure exerted at $r = \rho$, and can therefore be found as $p_* = pa^2/\rho^2$ (by direct substitution in Eq. (6)).

It follows that the by letting $r = \rho$ in Eq. (10) an analytical expression can be obtained for $u_+(\rho)$, which can then be substituted in Eq. (9) for the development of a second boundary condition, in addition to Eq. (5), at the active site/matrix interface, as

$$u_r(a) = \frac{pa^2}{E_g}\left\{\frac{1}{a} - \frac{2(1-v_g)}{\rho} + \frac{3(1-v_g)(b^3 - Sb\rho^2)}{2\rho(b^3-\rho^3)}\right\}, \tag{11}$$

where $S = qb^2/(pa^2)$.

Finally, the displacement at the outer matrix boundary $(r = b)$ is found by direct substitution in Eq. (10) as

$$u_r(b) = \frac{pa^2}{2bE_g}\left\{\frac{3(1-v_g)(b^2\rho - Sb^3)}{b^3-\rho^3} + S(1+v_g)\right\}. \tag{12}$$

Now we have all the parameters required in order to define the opening tensile stress responsible for crack growth and stability. Since the damaged zone can support only radial stresses, and hence it consists of radial cracks, the stress responsible for cracking, is $\sigma_{\theta\theta}$. In fact, Dempsey et al. [12] have found that for an axial configuration such as the one at hand, $\sigma_{\theta\theta}$ is given as

$$\sigma_{\theta\theta}(\rho^+) = \frac{pa^2}{b^2}\left[\frac{1-3S(\rho/b)^2+2(\rho/b)^3}{2(\rho/b)^2(1-(\rho/b)^3)}\right]. \tag{13}$$

Based on Ref. [12] the energy released as the crack grows can be defined as

$$G(\rho) = \frac{2(1-v_g)\rho\sigma_{\theta\theta}^2(\rho^+)}{nE_g}, \tag{14}$$

which in turn gives the stability index as

$$\kappa = \frac{b}{G}\frac{dG}{d\rho}. \tag{15}$$

It can be seen that in order to define the crack opening stress it is necessary to know what p and S are. Since the battery system is under equilibrium, self equilibrated loading conditions imply that $qb^2 = pa^2$, and hence $S = 1$. p can now be found by setting Eqs. (5) and (11) equal to each other, and solving for p, hence

$$p = \Delta\left\{\frac{a^2}{\rho E_g}\left[\frac{\rho}{a} - \frac{(1-v_g)}{2} - \frac{3(1-v_g)\rho^2}{2(b^2+b\rho+\rho^2)}\right] + \frac{(a+\Delta)1-2v_s}{E_s}\right\}^{-1}. \tag{16}$$

The calculations performed in the sequel are concerned with this self-equilibrated loading case.

4. Volume fraction considerations

In manufacturing electrodes with the aforementioned structure, it is of interest to examine the effect that the active site volume fraction has on crack initiation and propagation. In order to do so we must know the mechanical properties of the active sites. Upon Li-insertion in Si (and Sn) its crystal structure changes from cubic to tetragonal, hence the elastic modulus depends on Li-content. Experimental data providing the modulus of active sites as a function of Li content are not available, however, so in the sequel the values of the modulus for bulk Si will be employed; this is a valid approximation if one considers that the purpose of the present work is to illustrate how to apply the above formulation to obtain design criteria for Li-batteries. Moreover, the ancillary parameters are not available at this time for many of the well-known lithium ion conductors that may act as matrix materials. Thus example matrix materials exhibiting a variety of mechanical behaviors will be examined in order to develop specific design criteria for mechanical stability.

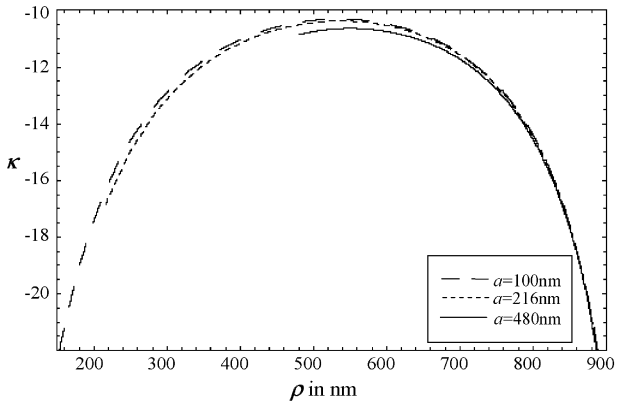

Fig. 3. Stability plots for systems with different active site volume fractions.

4.1. Stability index

In order to determine the size of the active sites that will result in a more stable battery system, we plot the stability index κ with respect to the crack radius ρ, for $b = 1\,\mu m$ and varying a. The various stability behaviors obtained are shown in Fig. 3. The active sites are taken to comprise of Si, while the matrix is of soda glass.

The more negative the values at which the stability curves start out the more stable the system, since a greater energy difference is required for crack growth to initiate. It can therefore be predicted from Fig. 3 that smaller active sites (i.e. smaller active site volume fractions f, where $f = a^3/b^3$ result in more stable anodes, since crack growth is initiated with greater difficulty for such systems.

4.2. Griffith's criterion

Based on Griffith's theory a crack will continue growing as long as the energy released (G) during its propagation is greater from the energy (G_c) required to create the new crack surface. By plotting therefore Eq. (14) together with the fracture energy (G_c) of the matrix material, which is a material constant, we can determine the crack radius at which the two energies intersect and hence estimate the distance at which crack growth will stop.

In Fig. 4 we therefore plot G for various active site volume fractions together with G_c. The active sites are taken to be Si, whereas the matrix is Y_2O_3. It can be seen that the smaller the volume fraction of the active sites the smaller the distance at which crack growth stops. Hence, it is again predicted that smaller volume fractions of the active sites are more stable since they allow for less cracking. Furthermore, by plotting G and G_c, for the same volume fractions (i.e. $a = 100\,nm$, $b = 1\,\mu m$), and active sites but different matrix materials, we can predict which matrix material allows for the smallest crack propagation distance before cracking ceases; the results re shown in Table 1, where it can be seen that the most preferable material, based on these considerations, is Y_2O_3 (that is why it as used in Fig. 4). It is noted that in the construction of Fig. 4, the number of radial cracks, n, present had to be assumed, as Eq. (14) suggests. To obtain accurate values, respective experiments must be

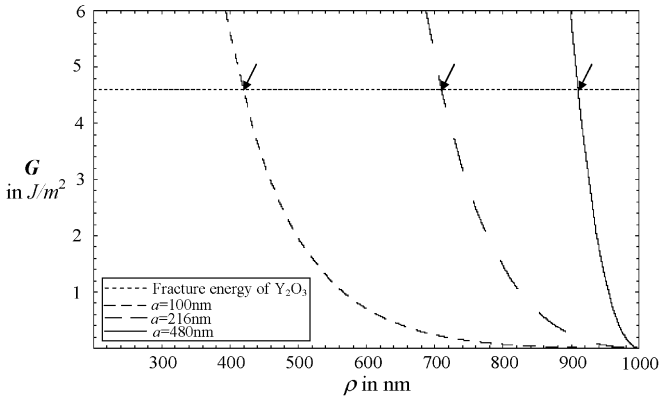

Fig. 4. Griffith's criterion for an electrode that comprises of Si active sites and Y_2O_3 matrix; various active site volume sites are considered. Arrows indicate the distance at which crack growth stops.

Table 1
Distance at which cracking stops for various matrix materials when $a = 100$ nm and $b = 1$ μm

Material	G_c (J m^{-2})	Critical crack radius ρ at which cracking stops (nm)
SrF_2	0.36	725
ThO_2	2.5	450
Y_2O_3	4.6	425
KCl	0.14	840

performed, since n, not only depends on the matrix material but it also changes according to ρ. Due to lack of such experimental data, however, and for illustration purposes, it is assumed that $n = 20$.

It should be noted that even if the actual Si elastic modulus value was employed in this section the qualitative patterns would remain the same, i.e. smaller active sites are more stable and hence crack growth initiation is more difficult, and they also allow for smaller crack distances and Y_2O_3 is the more preferable matrix from those considered in Table 1.

5. Critical crack length

In addition to the above volume fraction considerations and use of Griffith's criterion to determine when fracture will stop, direct use of the opening tensile stress Eq. (13), can provide information concerning the critical crack length at which fracture of the electrode will occur, as well as the size of the active sites that theoretically will result in no cracking. In particular, Eq. (13) gives us the tensile crack opening stress as a function of the crack radius (ρ), for any given material and geometric parameters. If, however, we set $\sigma_{\theta\theta}$ of Eq. (13) equal to the ultimate tensile strength of the matrix, and we define all the material and geometric parameters, the only unknown we are left with is ρ. Hence, we can solve numerically for ρ to obtain the critical crack radius and corresponding critical crack length ($\rho - a$) at which fracture of the electrode will take place for the corresponding system.

In particular, it is of interest to keep the geometric parameters the same, while we vary the material parameters so that we can obtain which material selections allow for the greatest critical crack lengths. Such a sample comparison is done in Table 2; again Si is used as the active site, hence $E_s = 112$ GPa and $\upsilon_s = 0.28$, while various ceramics which are inert with respect to Li are used as the matrix. Two limiting cases are examined: (i) $a = 10$ nm and $b = 1$ μm, i.e. the active site volume fraction is very small, (ii) $a = 750$ nm and $b = 1$ μm, i.e. the active site volume fraction is 0.42. It should be noted that the volume expansion of Si and Sn upon maximum Li insertion is approximately 300%; this corresponds to $\Delta = a^{1/3} - a$.

Unfortunately, the same materials could not be used for both Tables 1 and 2 since for the materials in Table 1 the ultimate tensile strength could not be found in the literature, while for the materials in Table 2 the critical fracture energy (G_c) could not be found. It can be seen from Table 2 that B_4C is the most preferable matrix material since it allows for the greatest critical crack radius and hence more electrochemical cycles can be performed before the electrode fractures. Furthermore, by comparing Sn and Si active sites it can be seen that the latter are more preferable because they result in a longer anode lifetime since they allow for greater crack lengths prior to fracture.

Furthermore, from Eq. (13) we can estimate the size of the active sites that will result in no cracking. When the crack radius (ρ) equals the radius of the active site (a) it implies that the crack length ($\rho - a$) is zero and hence no cracks are present. Therefore by defining the material parameters in Eq. (13), where again $\sigma_{\theta\theta}$ = ultimate tensile strength, setting $\rho = a$ and choosing a particular b we can estimate the corresponding radius a that will theoretically result in no cracking. Such sample results are shown in Table 3.

Table 2
Critical crack length for various ceramics (material parameters estimated from CRC Mater. Sci. Eng. Handbook [13])

Material	Ultimate tensile strength (MPa)	Elastic modulus (GPa)	Poisson's ratio	Critical crack radius ρ (nm) for active sites when $a = 10$ nm		Critical crack radius ρ (nm) for active sites when $a = 750$ nm	
				Si	Sn	Si	Sn
Al_2O_3	255	345	0.23	93	76	650.9	649.5
B_4C	155	450	0.21	123	99	651.6	650.9
BeO	246	400	0.24	97	78	651	649.8
WC	345	700	0.24	87	69	650.4	648.8
ZrO_2	175	140	0.23	95	81	651.3	650.4

Table 3
Active site size that results in no cracking when $b = 1$ μm

Material	Radius a (in nm) of active site that results in no cracking when $b = 1$ μm
Al_2O_3	757
B_4C	781
BeO	746
WC	745
ZrO_2	758

6. Conclusions

The present study was able to develop design criteria (based on a theoretical mechanical analysis) for nanocomposite active/inactive anodes for rechargeable Li-ion batteries. Particular conclusions are: (i) smaller active site volume fractions are preferable since they are more stable (i.e. crack growth initiation is more difficult), and they also allow for a smaller crack propagation distance to be attained before it is energetically favorable for crack growth to stop, based on Griffith's criterion. This theoretical prediction is consistent with the experimental evidence in Ref. [14], which shows that fibers comprised of nanospherical SnO_2 crystals can be cycled without a loss in capacity. (ii) Si active sites result in a greater anode lifetime (compared to Sn) since their use allows for more electrochemical cycles to be performed prior to fracture.

In general, it was illustrated that if the fracture energy (G_c) of the inactive material (i.e. matrix) is known, the distance at which cracking will stop can be obtained from Griffith's criterion, while the critical crack length at which fracture will take place can be estimated, through Eq. (13) if the ultimate tensile strength of the matrix is known. Furthermore, for a particular materials system the size of the active sites that will theoretically result in no cracking can be estimated. Hopefully, the present work will motivate experimentalists to look further into the mechanical properties of materials being used as inactive matrices, and also measure the modulus of Si (and other active site materials) as a function of Li content.

Acknowledgments

The support of the National Science Foundation through its Graduate Research Fellowship Program and to the European Commission under RTN/DEFINO HPRN-CT 2002-00198 (KEA) and the Grant OPP-0338226 (JPD) is gratefully acknowledged.

References

[1] J. Wang, I.D. Raistrick, R.A. Huggins, J. Electrochem. Sot. 133 (1986) 457.
[2] I.A. Courtney, J. Dahn, J. Electrochem. Sot. 144 (1997) 2045.
[3] M.M. Thackeray, C.S. Johnson, J.T. Vaughey, N. Li, S.A. Hackney, J. Mater. Chem. 15 (2005) 2257.
[4] L.Y. Beaulieu, K.W. Eberman, R.L. Turner, L.J. Krause, J.R. Dahn, Electrochem. Solid-State Lett. 4 (9) (2001) A137–A140.
[5] J. Graetz, C.C. Ahn, R. Yazami, B. Fultz, Electrochem. Solid-State Lett. 6 (9) (2003) A194–A197.
[6] K.E. Aifantis, S.A. Hackney, J. Mech. Behav. Mater. 14 (2003) 413.
[7] K.E. Aifantis, J.P. Dempsey, J. Power Sources 143 (2005) 203–211.
[8] B. Gao, S. Sinha, L. Fleming, O. Zhou, Adv. Mater. 13 (2001) 816–819.
[9] H. Li, X. Huang, L. Chen, Z. Wu, Y. Liang, Electrochem. Solid-State Lett. 2 (1999) 547.
[10] T. Takamura, S. Ohara, J. Suzuki, K. Sekine, Abstract 257, The 11th International Meeting on Lithium Batteries, Monterey, CA, June 23–28, 2002.
[11] H.M. Weestergard, Theory of Elasticity and Plasticity, Harvard University Press, 1953.
[12] J.P. Dempsey, L.I. Slepyan, I.I. Shekhtman, Int. J. Fract. 73 (1995) 233–261.
[13] CRC Mater. Sci. Eng. Handbook.
[14] N. Li, C.R. Martin, B. Scorsati, J. Power Sources 97-98 (2001) 240–243.